

MOL-010108

**MOLECULAR DETERMINANTS OF THE AGONIST BINDING DOMAIN OF A P2X RECEPTOR-
CHANNEL**

Zonghe Yan, Zhaodong Liang, Melanija Tomic, Tomas Obsil and Stanko S. Stojilkovic

Section on Cellular Signaling, Endocrinology and Reproduction Research Branch

National Institute of Child Health and Human Development

National Institutes of Health, Bethesda, Maryland 20892-4510 (Z.Y., Z.L., M.T., S.S.S.);

and Department of Physical and Macromolecular Chemistry, Faculty of Science

Charles University, Prague, Czech Republic (T.O.)

MOL-010108

Running Title: Ligand binding domain of P2XRs

Corresponding author:

Stanko S Stojilkovic
ERRB/NICHD
Bldg. 49, Room 6A-36
49 Convent Drive
Bethesda, MD 20892-4510
Tel: 301-496-1638
Fax: 301-594-7031
Email: stankos@helix.nih.gov

Number of text pages: 29

Number of Tables: 1

Number of words

Abstract: 167

Introduction: 714

Discussion: 1426

Abbreviations: P2XRs, P2 purinergic receptor-channels; P2YRs, P2 purinergic G protein-coupled receptors; $[Ca^{2+}]_i$, intracellular calcium concentration; GFP, enhanced green fluorescent protein; τ_{des} , the rate of receptor desensitization; 2-MeS-ATP, 2-methylthio ATP tetrasodium; BzATP, Benzoylbenzoyl-ATP; $\alpha\beta$ -meATP, $\alpha\beta$ -Methylene-ATP.

MOL-010108

P2X receptors (P2XRs) are a family of ligand-gated cation channels composed of two transmembrane domains, N- and C-termini located intracellularly, and a large extracellular loop containing the ATP binding domain. To identify regions important for binding and gating, previous experimental work was focused on mutagenesis of conserved ectodomain residues. Here we used the known sequence and secondary structure similarities between the Lys¹⁸⁰-Lys³²⁶ ectodomain region of P2X₄ and the class II aminoacyl-tRNA synthetases as a guide to generate a three-dimensional model of the receptor-binding site and to design mutants. The interplay between homology modeling and site-directed mutagenesis suggested that Asp²⁸⁰ residue of P2X₄R coordinates ATP binding via the magnesium ion, Phe²³⁰ residue coordinates the binding of the adenine ring of ATP, and Lys¹⁹⁰, His²⁸⁶ and Arg²⁷⁸ residues coordinate the actions of negatively charged alpha, beta, and gamma-phosphate groups, respectively. Until the crystal structure of the channel is solved, this model could provide a useful approach for future studies on identification of ATP binding domain and gating of P2XRs.

Introduction

P2X receptors (P2XRs) are a family of ATP-gated cation channels comprised of seven receptor subunits, termed P2X₁₋₇ (Ralevic and Burnstock, 1998; North, 2002). Each subunit is composed of two transmembrane domains, placing N- and C-termini intracellularly and most of the protein extracellularly (Newbolt et al., 1998). The trimeric homo- or heteromeric assembly of subunits organized in a head-to-tail orientation around the central pore most likely accounts for the formation of functional P2XRs (Nicke et al., 1998; Jiang et al., 2003). Among subunits the C-termini vary in their structure and length (North, 2002) and contain several motifs involved in receptor desensitization (Koshimizu et al., 1999). The ectodomain is glycosylated (Rettinger et al., 2000; Hu et al., 2002) and includes ten conserved cysteine residues, probably forming disulphide bonds and contributing to the tertiary structure of the receptor (Ennion et al., 2001; Clyne et al., 2002b). About 80 other extracellular residues are also conserved in at least six subunits. The ectodomain contains the ligand binding pocket and structural elements that influence receptor deactivation and desensitization rates (Fabbretti et al., 2004; Sokolova et al., 2004; Zemkova et al., 2004). The three-dimensional structure of P2XRs is unknown and it has not been determined whether ligand binding is inter- or intra-subunit. However, it is well established that the constituent components of ATP show no agonist or antagonist actions at P2XRs, indicating that both the adenine ring and the triphosphate chain are critical for high affinity binding (North, 2002). It is also established that P2XRs are regulated allosterically by protons, divalent cations and metals (Li et al., 1997; Wildman et al., 1999; Clarke et al., 2000; Negulyaev and Markwardt, 2000; Clyne et al., 2002a; Coddou et al., 2003).

At the present time, there are two models that describe ATP binding site at P2XRs. Evans and collaborators developed a model of ATP binding pocket based on data from site-directed mutagenesis of human P2X₁R (Vial et al., 2004). Mutation of aromatic amino acids at this receptor indicated the relevance of two residues, F185 and F291, in ATP action (Roberts and Evans, 2004). This finding is consistent with a hypothesis that adenine moiety of an ATP molecule is sandwiched between these two residues, similar to that observed in crystal structure of 5'-nucleotidase (Knofel and Strater, 2001). Furthermore, three conserved positively charged residues, K68, R292, and K309, that are close to the vestibule of the ionic pore, appear to be associated with the binding of the phosphate chain of ATP

(Ennion et al., 2000). This model does not include a role of Mg^{2+} in coordination of ATP binding (Vial et al., 2004), as experimental data revealed no effects of mutation of numerous negatively charged residues on ATP potency (Ennion et al., 2001).

Freist and collaborators developed a theoretical model of ATP binding site, which is based on sequence alignments and secondary structure predictions between class II aminoacyl-tRNA synthetases and P2XRs (Freist et al., 1998). This model has not been experimentally tested, presumably because the sequence alignment between the enzyme and P2XRs is relatively poor. However, several residues predicted by sequence alignment to participate in ATP binding have been mutated in studies on conserved residues in ectodomains of human P2X₁ and rat P2X₂ subunits. Consistent with the model, mutation of K188 at P2X₂R, the corresponding residue for recognition of γ -phosphate, produced a rightward shift in the sensitivity of receptors to ATP (Jiang et al., 2000). Furthermore, the responsiveness to ATP was abolished by mutation of F227, the potential residue for adenosine recognition (Nakazawa et al., 2004). At P2X₁R, mutation of K190 also produced a rightward shift in the sensitivity, whereas ATP potency was not affected by substitution of R314, the potential residue for recognition of γ -phosphate (Ennion et al., 2000), and F230, the potential residue for adenosine recognition (Roberts and Evans, 2004).

Here we tested Freist's model by mutating K190, K197, F230, D280, and R318 residues of rat P2X₄R. Using the crystal structures of several class II aminoacyl-tRNA synthetases as templates, we also built a three-dimensional model of K180-K326 ectodomain region of P2X₄, and identified and mutated additional four residues that could participate in ATP binding. The interplay between homology modeling and mutagenesis indicates which residues participate in ATP binding at P2X₄R and provides a useful framework for identification of ligand binding pocket at other subunits.

Materials and Methods

DNA constructs, site-directed mutagenesis, cell culture, and transfection. The C-terminal GFP-tagged P2X₄ construct was generated through deleting sequences between the C-terminus of coding sequences of subcloned P2X₄ cDNA and the initiation codon of GFP gene in the previously described P2X₄-biscistronic enhanced fluorescent protein expression vector (pIRES2-EGFP) construct (He et al., 2003b), mainly including the internal ribosome entry site (IRES). Deletion was created using the QuikChange[®] XL site-directed mutagenesis kit (Stratagene) according to the manufacturer's instructions and 5'-ctttcgggggagatgaaccagatggtgagcaagggcgaggag-3', 5'-ctcctcgccttgctcaccatctggtcatctccccgaaag-3' as the mutagenic oligonucleotide primers, synthesized and PAGE purified by IDT[®] (Integrated DNA Technology, Coralville, IA). Both the C-terminal GFP-tagged P2X₄ and P2X₄/pIRES2-EGFP construct were used as templates for production of plasmids containing the specific amino acid residue point mutation of P2X₄ cDNA. The point mutations were introduced using the QuikChange[®] XL site-directed mutagenesis kit. Productions of the correct C-terminal GFP-tagged P2X₄ constructs, mutations and absence of coding errors in these constructs were verified by dye terminator cycle sequencing (PerkinElmer Life Sciences, performed by Veritas, Inc., Rockville, MD). Large-scale plasmid DNAs were prepared using a QIAfilter[™] Plasmid Maxi kit (Qiagen). Mouse immortalized gonadotropin-releasing hormone-secreting GT1-7 cells and human embryonic kidney HEK293 cells were used for expression of wild type and mutant P2X₄ receptors, as described previously (He et al., 2003a). GT1-7 and HEK293 cells were routinely maintained in Dulbecco's modified Eagle's medium/Ham's F12 medium (1:1) containing 10% (v/v) fetal bovine serum (Biofluids, Rockville, MD) and 100 µg/ml gentamicin (Invitrogen) in a water-saturated atmosphere of 5% CO₂ and 95% air at 37 °C. Cells were plated on 25-mm poly-L-lysine (0.01% w/v; Sigma)-coated coverslips at a density of 0.1 x10⁶ cells for current recording and 0.5 x10⁶ cells for calcium measurement per 35-mm dish. The transient transfection was conducted 24 h after plating the cells using 2 µg of DNA and 5 µl of LipofectAMINE 2000 reagent (Invitrogen) in 2 ml of serum-free Opti-MEM. After 4.5 h of incubation, the transfection mixture was replaced with normal culture medium. Cells were subjected to experiments 24-48 h after transfection.

Calcium measurements. Transfected GT1-7 cells were preloaded with 1 μ M Fura-2 acetoxymethyl ester (Fura-2/AM; Molecular Probes, Eugene, OR) for 60 min at room temperature in Modified Krebs-Ringer buffer (in mM): 120 NaCl, 5 KCl, 1.2 CaCl₂, 0.7 MgSO₄, 15 HEPES, and 1.8 g/liter glucose (pH 7.4). After dye loading, cells were incubated in Modified Krebs-Ringer buffer and kept in the dark for at least 30 min before [Ca²⁺]_i measurements. Coverslips with cells were mounted on the stage of Eclipse TE 200 microscope (Nikon, Japan) attached to the PTI[®] IC-300 fluorescence system (Photon Technology International, Lawrenceville, NJ). Cells were stimulated with various doses of agonists, the dynamic changes of [Ca²⁺]_i were examined under a x40 oil immersion objective during exposure to alternating 340- and 380-nm excitation light beams, and the intensity of light emission at 520 nm was measured. The F₃₄₀/F₃₈₀ ratio of light intensities, which reflects changes in [Ca²⁺]_i, was simultaneously followed in 15 to 50 cells. Cells expressing GFP were optically detected by an emission signal at 520 nm when excited by a 488-nm light. Experiments were done in cells with comparable GFP fluorescence signals (about 5 arbitrary units at 0-10 scale), and no repetitive stimulation was done to avoid the possible impact of desensitization on the amplitude and pattern of [Ca²⁺]_i signals.

Current measurements. Electrophysiological experiments were performed on HEK293 cells at room temperature using whole-cell patch clamp recording techniques. ATP-induced currents were recorded using an Axopatch 200B patch clamp amplifier (Axon Instruments, Union City, CA) and were filtered at 2 kHz using a low pass Bessel filter. Patch electrodes, fabricated from borosilicate glass (type 1B150F-3; World Precision Instruments, Sarasota, FL) using a Flaming Brown horizontal puller (P-87; Sutter Instruments, Novato, CA), were heat-polished to a final tip resistance of 4-6 megaohms. All current records were captured and stored using the pClamp 8 software packages in conjunction with the Digidata 1322A A/D converter (Axon Instruments). In general accordance with literature (Jiang et al., 2003), patch electrodes were filled with a solution containing (in mM): 142 NaCl, 1 MgCl₂, 10 EGTA, and 10 HEPES; the pH was adjusted with 10 M NaOH to 7.35. The osmolarity of the internal solutions was 306 mOsm/l. The bath solution contained (in mM): 142 NaCl, 3 KCl, 1 MgCl₂, 2 CaCl₂, 10 glucose, and 10 HEPES; the pH was adjusted to 7.35 with 10 M NaOH. The osmolarity of this solution was 295-305 mosM. ATP was daily prepared in bath buffer with pH properly re-adjusted and applied using a fast gravity-driven

microperfusion system (BPS-8, ALA Scientific Instruments, Westbury, NY). The current responses were recorded from single spherical cells clamped at -60 mV. The impact of expression level on current was reduced by selecting cells with comparable P2X₄ fused GFP fluorescence before immersing the electrode in bath solution for gigaohm seal. Responses were normalized to cell membrane capacitance (in a range of 7-23 pF) and presented as current density (in pA/pF). Dose-response data were collected from recordings of a range of ATP concentration buffers applied to single cells with a washout interval of 5 minutes between each application, and the corresponding currents were normalized to the highest current amplitude. The pH sensitivity of receptors was tested by repetitive application of ATP at pH 6.50, 7.35 and 8.00, with pH buffer equilibration for 1 minute before agonist application.

Confocal microscopy. The distribution of GFP-tagged receptors within live cells was examined by laser scanning confocal microscopy. HEK293 cells were cultured on poly-L-lysine coated coverslips (0.1×10^6 cells/dish), transfected and imaged the next day. The culturing medium was replaced with phenol red and ATP-free Krebs-Ringer buffer and coverslips with cells were mounted on a stage of inverted microscope (Nikon Diaphot 300) attached to a Bio-Rad MRC 1024 system (Bio-Rad, Hercules, CA). Images were collected under 60 x objective and further zoom (3 x) was also applied.

Modeling of P2X ectodomain. Three-dimensional model of rat P2X₄-K¹⁸⁰-K³²⁶ ectodomain region was generated using the SWISS-MODEL server (Schwede et al., 2003) and crystal structures of seryl-tRNA synthetase (PDB code 1SES), glycyl-tRNA synthetase (PDB code 1B76), and histidyl-tRNA synthetase (PDB code 1KMN) as templates (Belrhali et al., 1994; Arnez et al., 1999; Arnez et al., 1997). The secondary structure of rat P2X₄ sequence was predicted using the PSI-PRED algorithm (Jones, 1999). Sequence and secondary structure homology between P2XRs and the class II aminoacyl-tRNA synthetases (Freist et al., 1998) was used to build a three-dimensional model of rat P2X₄-K¹⁸⁰-K³²⁶ ectodomain region using the DeepView/Swiss-PdbViewer v3.7 program (Guex and Peitsch, 1997). The final model was validated by PROCHECK and bad contacts were corrected manually by O program (Jones et al., 1991). Disulphide bridges Cys²¹⁷-Cys²²⁷ and Cys²⁶¹-Cys²⁷⁰ were created using O program. Resulting model was then energy minimized using GROMACS package (www.gromacs.org) with the

parameters set ffG43a1. The ligand docking started with manual docking of ATP molecule into the predicted binding site of rat P2X₄ K¹⁸⁰-K³²⁶-ectodomain model based on homology with class II aminoacyl-tRNA synthetases. Subsequently, the geometric recognition algorithm implemented in the docking program GRAMM (Katchalski-Katzir et al., 1992) and GHEMICAL modeling package (Hassinen and Perakyla, 2001) were used to refine the structure of P2X₄-ATP complex.

Calculations. Whenever appropriate, the data were presented as mean ± SEM. The time course of the current and [Ca²⁺]_i was fitted by one phase exponential decay function ($ae^{-kt} + b$; where $k = 1/\tau_{des}$) using pClamp 8 program (Axon Instruments) and GraphPad Prism 4 (GraphPad Software, San Diego, CA), respectively. Significant differences, with $p < 0.01$, were determined by Mann-Whitney test using GraphPad InStat 3.05. Concentration-response data were fitted by a four-parameter logistic equation using a nonlinear curve-fitting program that derives EC₅₀ values (Kaleidagraph; Synergy Software, Reading, PA).

Results

Experimental considerations. To visualize the expression pattern of wild type and mutant P2X₄Rs, the sequence for enhanced GFP was tagged to the C-terminal of P2X₄R as described in Material and Methods and both fused and non-fused receptors were expressed in HEK293 and GT1-7 cells. As shown in Fig. 1A, left panel, GFP translated from the same bicistronic mRNA as P2X₄R was homogeneously distributed within the HEK293 cells. The P2X₄R-fused GFP was also expressed, but was localized in the plasma membrane and in intracellular structures, presumably Golgi apparatus and vesicles (Fig. 1A, right panel). Consistent with the plasma membrane-expression of P2X₄-GFP in HEK293 cells, ATP in 0.5 μM to 100 μM concentration range always triggered an inward current in GFP-positive cells. Figure 1B shows typical current traces elicited by 100 μM ATP in five cells expressing P2X₄R (left panel) and five cells expressing the GFP-tagged P2X₄R (right panel). These and all other experiments were done in cells with comparable GFP fluorescence signals (about 5 arbitrary units at 0-10 scale). There was no obvious difference in the rise time and peak amplitude of current responses (labeled as *I* in Fig. 1B) between two receptors. Also, in all cases mono-exponential decays of current were observed with highly comparable time constants of desensitization (labeled as τ_{des} in Fig. 1 B).

In further experiments, we analyzed the patterns of calcium signaling by two receptors. HEK293 cells endogenously express calcium-mobilizing P2Y receptors and their co-activation interferes with calcium influx-dependent signaling (He et al., 2003a). To avoid this, we used GT1-7 neurons, which do not express P2XR or P2YRs endogenously (Koshimizu et al., 1998). The patterns of calcium signaling by two receptors were highly comparable independently of the status of voltage-gated Ca²⁺ influx. Figure 1C illustrates typical pattern of the rise in intracellular calcium concentration ($[Ca^{2+}]_i$) in cells without blockade of voltage-gated Ca²⁺ influx. The rise times and average peak amplitudes of calcium signals were similar, as well as the time constants of calcium signal desensitization during continuous application of ATP. Finally, concentration-dependent studies using current (Fig. 1D) and calcium (not shown) measurements revealed that the potency of ATP for two receptors was similar. All together, these results indicate that the attachment of GFP does not obviously affect receptor expression and pharmacological and kinetic properties, but provides a useful method to clarify the plasma membrane expression of protein.

Characterization of mutants predicted by Freist's alignment model. In Freist's model, the highly conserved K190 residue of P2X₄R accounts for binding of the α -phosphate moiety of ATP, whereas K197 and R318 participate in binding of the γ -phosphate moiety of ATP. The relevance of these residues was tested by generating the following mutants of P2X₄ subunit: K190A, K190R, K197A, R318A, and R318K. The K197A mutant was functional and ATP potency and the rate of receptor desensitization were not obviously affected (Table 1). In contrast, three out of eleven cells expressing K190A mutant did not respond to application of 100 μ M ATP (Fig. 2B), whereas the residual cells responded with peak current representing about 1% of that observed in controls (Table 1). A decrease in responsiveness of this mutant did not result from trafficking problems, as receptor exhibited typical pattern of plasma membrane expression (Fig. 2A). Also, a fraction of mutated receptors not fused with GFP did not respond to 100 μ M ATP application, whereas the residual cells responded with low amplitude signals (not shown). All cells expressing K190A mutant responded to 5 mM ATP with higher current amplitude (Fig. 2C), but not to application of 100 μ M 2-MeS-ATP and BzATP (not shown), indicating a rightward shift in the sensitivity of receptors to agonists. The receptor function was preserved in K190R mutant (Fig. 2B), confirming the importance of a positively charged residue at this position. As shown in Fig. 2D, the K190R receptor responded to ATP application in a dose-dependent manner, with an EC₅₀ value shifted slightly rightward from the control EC₅₀ (Table 1). The peak amplitude of K190R current induced by 100 μ M ATP was about 50% of the wild type channel, whereas the rates of receptor desensitization were not influenced (Table 1).

The plasma membrane expression pattern of R318A mutant was normal (Fig. 3A). However, the receptor showed a significant reduction in the peak current when stimulated with 100 μ M ATP (Fig. 3B&C; Table 1). Dose-dependent studies revealed a 20-fold decrease in the potency of ATP for mutant receptor compared to the wild type receptor (Fig. 3D). The relevance of a positively charged residue at this position was further indicated by replacement of arginine with lysine. The potency of ATP for R318K mutant was slightly shifted leftward (Fig. 3D), whereas the peak current amplitude was not significantly different from that observed in wild type channels (Fig. 3B&C, Table 1). Change in ATP potency reflects the amount of ATP required to induce the channel opening, but does not clarify which step in activation of receptors, a decrease in the binding affinity of receptor and/or the functional translation of agonist binding

to the gating, accounts for this shift. However, partial agonist may be able to discriminate between mutations that affect agonist binding versus P2XR-channel gating (Roberts and Evans, 2004). For P2X₄R, $\alpha\beta$ -meATP acts as a partial agonist (Khakh et al., 1999). As shown in Fig. 3E, the peak amplitude of current response of wild type P2X₄R to 1 mM $\alpha\beta$ -meATP was about 40% of that observed in response to stimulation with 100 μ M ATP. Furthermore, the wild type and mutant channels showed similar EC₅₀ values when stimulated with $\alpha\beta$ -meATP (Fig. 3F). These observations are more consistent with the role of R318 residue in signal transduction than agonist binding.

The predicted residue by Freist's model for Mg²⁺ binding at P2X₄R is D280. To neutralize the negative charge of this residue, we generated two mutants, D280A and D280Q. Both mutants were expressed at the plasma membrane in a manner highly comparable to that observed with wild-type receptors (Fig. 4A&B, left panels). Mutants also responded to application ATP, but with a small current (Fig. 4A&B, central and right panels). The peak current amplitude induced by 100 μ M ATP represented about 4% of that seen with wild-type receptors. Increase in ATP concentrations up to 5 mM only slightly (2-3 fold) increased the amplitude of current (Fig. 4A&B, right panels). In concentrations above 5 mM, ATP permeabilized cells independently of the expression of P2XRs. When added in 100 μ M concentrations, BzATP and 2-MeS-ATP induced currents of comparable amplitudes and profiles as 100 μ M ATP. Similar results were observed with mutant receptors not tagged to GFP, as well as in GFP-tagged and non-tagged mutant receptors when expressed in GT1-7 cells (not shown).

To further test the relevance of a negatively charged residue at this position for ATP action, we generated the "rescue" D280E-P2X₄ mutant. As shown in Fig. 4C, left panels, this mutant expressed in HEK293 cells responded to ATP stimulation with a current similar to that observed in cells expressing wild type channels. The mutant receptor also responded to 100 μ M ATP with a rise in [Ca²⁺]_i when expressed in GT1-7 cells (Fig. 4C, central panel). At 100 μ M ATP concentration, the peak of current signals was lower compared to the wild type receptor, but the rate of receptor desensitization was not affected (Table 1). The dose-response studies revealed typical pattern of response (Fig. 4C, right panel), with an estimated EC₅₀ value comparable to that observed in cells expressing wild type receptors (Table 1).

According to Freist's alignment model, F230 should play a role at P2X₄R in recognition of adenine group of ATP. Consistent with this prediction, F230A mutant of P2X₄R showed a small (less than 2-3% of

MOL-010108

that observed in controls) peak current response in 15 out of 17 GFP-positive cells stimulated with 100 μ M ATP (Fig. 5B&C, Table 1). Similar pattern of response was observed during application of 100 μ M 2-MeS-ATP and BzATP. The low responsiveness of this mutant did not result from its miss-expression, as it is indicated by localization of GFP fluorescence at the plasma membrane (Fig. 5A). Elevation in ATP concentrations to up to 5 mM was associated with increase in the peak current amplitude (Fig. 5C), further indicating the functional assemble of mutant subunits at the plasma membrane. Because of the non-specific effects of milimolar ATP concentrations, we were unable to estimate the EC₅₀ values for this mutant. The replacement of phenylalanine with tryptophan and tyrosine “rescued” the function of channels, indicating the importance of an aromatic residue in that position (Fig. 5D&E). The amplitude of current response by F230W and F230Y mutants was about 80% of that observed in wild type channels, whereas the rates of current desensitization for these two mutants were not affected (Table 1). Both mutants responded to ATP in a typical dose-dependent manner (Fig. 5F), with EC₅₀ values comparable to that observed in cells expressing wild type channels (Table 1).

Three-dimensional model of P2X₄R. We used several X-ray structures of aminoacyl-tRNA synthetases as templates for three-dimensional homology modeling of the 180-326 P2X₄ ectodomain fragment. As shown in Fig. 6A, the class II enzymes posses a unique fold with a catalytic domain built on a six-stranded antiparallel β -sheets surrounded by α -helices and contain three homologous sequences, termed motifs 1, 2 and 3 (Eriani et al., 1995). Three amino acid residues at motif 2 and one residue at motif 3 form an ATP binding site (Arnez et al., 1997). Our model of the P2X₄R 180-326 fragment also adopts a six-stranded β -pleated sheet structure and contains an ATP binding site (Fig. 6B). However, the molecule of ATP docked within the ligand-binding site of P2X₄ ectodomain model adopts more extended conformation compared to the class II aminoacyl-tRNA synthetases. Also, notice the difference in lengths of a large loop between β 1 and β 2 strands and the α -helix between β 2 and β 3 strands in the sequences of the enzyme and P2X₄R (Fig. 6B).

The details of the enzyme’s ATP binding pocket are shown in Fig. 6C&E. The adenine base of ATP stacks over the invariant phenylalanine residue from motif 2, the α -phosphate interacts with the first conserved arginine of motif 2, while the second highly conserved arginine of motif 2 and the completely

MOL-010108

conserved arginine of motif 3 interact with the γ -phosphate. The predicted ligand-binding pocket of P2X₄R incorporates three of five residues indicated by Freist's alignment model: D280, F230, and K190. ATP is cradled by the antiparallel β -sheets and the adenine base stacks over the F230 residue (Fig. 6D&F). The aspartate 280 of β 4 strand binds to the magnesium ion, which is modeled between this residue and the γ -phosphate group of ATP. This interaction mimics the binding of D293 to the magnesium ion of an ATP-Mg²⁺ complex in the enzyme structure. The K190 residue of P2X₄ subunit located within the strand β 1 interacts with the α -phosphate.

Contrary to Freist's alignment model, in our three-dimensional model the β 4 strand residue R278 interacts with the γ -phosphate, and the H286 residue located on the beginning of β 5 strand, and/or nearby K258 or N287 residues, interacts with the β -phosphate group of ATP. The difference in the length of a large loop between β 1 and β 2 strands in the sequences of the enzyme and channel underlies a shift of residues contributing to the recognition of the phosphate chain of ATP (Fig. 6B). This provides a rationale for the lack of effects of K197A mutation on the channel function (Table 1). The last P2X₄ residue predicted by Freist's model to be in close proximity of ATP is R318. However, our model indicates that, if R318 residue participates in ligand binding, it could be in the contact with deoxyribose ring rather than with γ -phosphate of ATP (Fig. 6D&F). The incorporation of this residue in α -helix is also consistent with our observation on the potential role of this segment in transduction of signaling toward the second transmembrane domain (Fig. 3). Finally, our model includes two disulphide bridges: the Cys²¹⁷-Cys²²⁷ and Cys²⁶¹-Cys²⁷⁰ (shown in orange in Fig. 6D). No large structural changes were necessary to create these bridges, as both pairs of cysteines were located close to each other. This provides another indication that the 180-326 fragment of P2X₄R ectodomain adopts the suggested β -pleated sheet fold.

Characterization of mutants predicted by three-dimensional model. To test the validity of the three-dimensional model predictions for the roles of R278 in γ -phosphate binding and H286, K258, and/or N287 residues in β -phosphate coordination, these amino acids were mutated and mutants were characterized. Experiments with R278A and R278K mutants supported the relevance of this residue in ATP binding. As shown in Fig. 7A, the R278A mutant was expressed at the plasma membrane (left panel), and responded

MOL-010108

to application of 100 μ M ATP (central-left panel), 2-MeS-ATP, and BzATP (not shown) with a small current. The rightward shift in the sensitivity of R278A receptor to ATP probably accounted for a decrease in peak current response, as there was an increase in current amplitude when cells were stimulated with 5 mM ATP (Fig. 7A, central-right panel). The replacement of arginine with lysine gave a functional channel, responding to ATP in a micromolar concentration range (Fig. 7A, right panel) and with an estimated EC_{50} value shifted slightly leftward from EC_{50} of wild type channels (Table 1). The peak current amplitude of mutant channel was significantly reduced (Fig. 7A, central-left panel, Table 1), whereas the rate of receptor desensitization was not affected (Table 1).

Mutation of K258 and N287 to alanine did not affect the function of channels, as illustrated by EC_{50} values, peak current responses, and rates of receptor desensitization (Table 1). In contrast, experiments with rat P2X₄R expressed in HEK293 cells confirmed effects of external pH on signaling. Changing the external pH from 7.35 to 6.5 reduced the peak current amplitude, whereas an increase in pH to 8 enhanced it (Fig. 7B, left bottom panel). The H286A-P2X₄ mutant was functional when expressed in HEK293 cells, and exhibited similar sensitivity to ATP as wild type channels (Fig. 7B, right panel), that is consistent with literature data (Xiong et al., 2004). The rate of mutant receptor desensitization was comparable to wild type channel (Table 1) when experiments were performed in cells bathed in pH 7.35 medium. Furthermore, there was no change in the current amplitude with changes in extracellular pH, in contrast to the wild type channel. Figure 7B, left upper panel, shows typical traces of current responses by mutant receptor stimulated with 3 μ M ATP, and Fig. 7B, central panel, shows the lack of effects of acidification on peak current in H286A mutant, confirming that pH sensitivity resides in the rat P2X₄ channel protein.

Discussion

The extracellular loop of P2XRs contains a sequence stretch in positions 170 to 330 that exhibits similarities with the catalytic domains of class II aminoacyl-tRNA synthetases (Freist et al., 1998). From this sequence alignments and secondary structure predictions, five residues emerged as potentially relevant for ATP binding at P2XRs: K190, K197, F230, D280, and R318 (P2X₄ counting). Here we show that mutation of three of these residues, K190, F230 and D280, severely affected P2X₄R function, supporting this model. The behavior of two P2X₂R mutants is also consistent with the model. However, of P2X₁R-R314, the potential residue for recognition of γ -phosphate (Ennion et al., 2000), and F230, the potential residue for adenosine recognition (Roberts and Evans, 2004), did not affect the efficacy of ATP for P2X₄R. Our experimental data also do not support a role of K197 in ATP action and question a role of R318 in ATP binding. A partial agreement of experimental data with Freist's model prompted us to build a three-dimensional model of P2X₄R. According to our model, the 180-326 fragment of rat P2X₄ ectodomain adopts a six-stranded antiparallel β -pleated sheet structure and contains the ATP binding site. As discussed below, our model also provided a rationale for the observed compatibility and differences between Freist's alignment model and the majority of experimental observations.

Many ATP-binding proteins bind ATP complexed with magnesium cations, which usually stabilize the conformation of ATP and/or represent structural parts of the active site and participate in catalysis. Therefore, negatively charged amino acids are often found to participate in ATP binding via this cation, including II aminoacyl-tRNA synthetases (Arnez et al., 1997). In Freist's alignment model the corresponding residue for Mg²⁺ binding at P2X₄R is D280 and in our three-dimensional model this residue is an integral component of ATP binding pocket. The relevance of this negatively charged residue on ATP-induced currents in other P2XRs has not been studied previously. We may speculate the broader relevance of negatively charged residues among channels because five receptors have aspartic acid at the corresponding position, whereas the corresponding residue at P2X₁R and P2X₆R is glutamic acid. In II aminoacyl-tRNA synthetases, both the aspartic and glutamic acid residues at the corresponding position mediate the recognition of ATP-Mg complex. In both classes of these enzymes, the stabilizing role of magnesium is best exemplified by the two ions, bridging the β - and γ -phosphates (Arnez et al., 1999). In non-physiological concentrations (2 to 10 mM), Mg²⁺ exhibits additional effects on ATP-induced

P2X₄R current. It inhibits ATP-gated ion channel function by decreasing the affinity of the agonist binding (Li et al., 1997), an effect probably resulting from changing the balance between positive and negative charges at the ligand-binding pocket. Single channel recording from cells expressing P2X₄R also showed inhibitory effects of high [Mg²⁺] in reducing the amplitude of single channel current, an observation consistent with a fast channel block, and reducing the mean opening time, suggesting an effect on ion gating (Negulyaev and Markwardt, 2000).

In general, positively charged ectodomain residues could interact with negative phosphate groups of ATP and coordinate the binding of the phosphate chain of this agonist. Both the alignment and three-dimensional models predict a role of K190 in recognition of α -phosphate. Experiments with P2X₁R (Ennion et al., 2000), P2X₂R (Jiang et al., 2000) and P2X₄R (present data) are in general agreement with this prediction. On the other hand, there is a large loop between β 1 and β 2 strands in the channel sequence in our model, whereas the class II aminoacyl-tRNA synthetases possess just a relatively short loop between these two strands. The extension of this loop misplaces the K197 residue and its function is substituted by β 4 strand residue R278. Consistent with the model prediction, mutation of the K197 residue did not affect ATP potency at P2X₄R, whereas R278A mutant, but not R278K mutant, showed a dramatic decrease in the sensitivity to ATP. Furthermore, the three-dimensional model indicates a role of H286 in ATP binding, whereas Freist's model does not identify a residue for recognition of β -phosphate group. The H286 residue is unique for P2X₄R. Earlier studies have indicated that acidification causes a rightward shift in the ATP concentration-response curves for P2X₄R (Wildman et al., 1999) and that mutation of H286 residue of the human P2X₄R completely abolished the pH sensitivity of this receptor at all agonist concentrations when the *Xenopus* oocyte expression system was used (Clarke et al., 2000). Our results with rat H286-P2X₄R mutant are consistent with these findings.

In addition, Freist's model suggests that the R318 residue of P2X₄R together with K197 residue participates in coordination of the γ -phosphate moiety of ATP. In our three-dimensional model, however, R318 residue is located just next to the H286 residue and could be in contact with deoxyribose ring of ATP. Moreover, R318 is an integral residue of the α -helix directed toward the second plasma membrane domain (Fig. 6B) and could participate in molecular signal transduction from ATP binding pocket toward the second transmembrane domain. As recently revealed, this could be relevant for conformation

changes in the pore that occur during receptor activation (Li et al., 2004). Experiments with $\alpha\beta$ -meATP, a partial agonist for P2X₄R, are in general agreement with the second hypothesis, but additional studies are needed to clarify this issue. Finally, of the potential interest for discussion is the diversity in the structure and length of the chain between F276 and Y292 (P2X₄ numbering) among P2XRs. In our model, this region of P2X₄R accounts for the parts of β 4 and β 5 strands and the interconnecting loop and contains three of five residues involved in ATP binding. We may speculate that such variability in the sequence structure reflects on agonist specificity and efficacy among receptors.

The site of detection of the adenine group gives nucleotide selectivity to the P2XRs and in many ATP binding proteins aromatic amino acids mediate the recognition of this group. For example, phenylalanine coordinates the recognition of adenine group of ATP by DEAD box helicases (Tanner et al., 2003). The Freist's alignment model suggested a role for F230 residue at P2X₁R and P2X₄R and the corresponding F227 residue at P2X₂R in coordination of adenine ring. The relevance of these two residues was tested at P2X₁R and P2X₂R and gave the opposite results; there was no change in ATP-induced current in F230A-P2X₁R mutant compared to wild type channels (Roberts and Evans, 2004), whereas the responsiveness to ATP was abolished in F227L-P2X₂R and F207I-P2X₂R mutants (Nakazawa et al., 2004). We also observed dramatic effects of F230 mutation at P2X₄R and this residue appears to be sufficient in coordination of binding of adenine ring. Single aromatic residues also coordinate the binding of adenine ring in class II aminoacyl-tRNA synthetases (Arnez et al., 1997) and P-type ATPases (Toyoshima and Mizutani, 2004). Multiple sequence alignment of P2XR channels shows that subunits other than P2X₁ contain a basic residue (R or K) just next to F230, whereas P2X₁ sequences have N, S, or Q residues at this position. This could account for differences in experiments with site-directed mutagenesis.

As discussed recently (Vial et al., 2004), mutagenesis may change the ATP potency (indicated by changes in EC₅₀ values), the response amplitude and/or the time course, but may also result in loss of function. Changes in EC₅₀ values may reflect changes in the ATP binding affinity, whilst changes in gating/channel properties of the receptors may reflect on the time-course of responses, i.e., activation, deactivation, and desensitization kinetics. On the other hand, the trafficking of receptors or the proper assemble of subunits at the plasma membrane may affect the amplitude of response or underlie the loss

MOL-010108

of function. In mutation studies, the GFP-tagged P2X₄ and confocal microscopy was used to identify their expression pattern in HEK293 cells. We believe that GFP fluorescence at the plasma membrane and the parallelism in the behavior of GFP-tagged and non-tagged receptors expressed in HEK293 and GT1-7 cells provides sufficient qualitative information about the plasma membrane expression of mutants and that a decrease in receptor function reflects the potential importance of targeted residues for ATP binding and/or gating rather than the problems in trafficking of receptors. This conclusion was further supported by previously published finding that a conserved motif in the cytoplasmic C termini of P2X subunits that is necessary for their plasma membrane expression (Jiang et al., 2003), and by our finding that preservation of charged or aromatic residues “rescued” the channel function. To this end, all mutant receptors responded to ATP when applied in a low millimolar concentration range, indicating that mutant subunits form functional plasma membrane channels but with low sensitivity to ATP.

References

- Arnez JG, Augustine JG, Moras D and Francklyn CS (1997) The first step of aminoacylation at the atomic level in histidyl-tRNA synthetase. *Proc Natl Acad Sci U S A* **94**:7144-7149.
- Arnez JG, Dock-Bregeon AC and Moras D (1999) Glycyl-tRNA synthetase uses a negatively charged pit for specific recognition and activation of glycine. *J Mol Biol* **286**:1449-1459.
- Belrhali H, Yaremchuk A, Tukalo M, Larsen K, Berthet-Colominas C, Leberman R, Beijer B, Sproat B, Als-Nielsen J, Grubel G and et al. (1994) Crystal structures at 2.5 angstrom resolution of seryl-tRNA synthetase complexed with two analogs of seryl adenylate. *Science* **263**:1432-1436.
- Clarke CE, Benham CD, Bridges A, George AR and Meadows HJ (2000) Mutation of histidine 286 of the human P2X4 purinoceptor removes extracellular pH sensitivity. *J Physiol (Lond)* **523 Pt 3**:697-703.
- Clyne JD, LaPointe LD and Hume RI (2002a) The role of histidine residues in modulation of the rat P2X(2) purinoceptor by zinc and pH. *J Physiol (Lond)* **539**:347-359.
- Clyne JD, Wang LF and Hume RI (2002b) Mutational analysis of the conserved cysteines of the rat P2X2 purinoceptor. *J Neurosci* **22**:3873-3880.
- Coddou C, Morales B, Gonzalez J, Grauso M, Gordillo F, Bull P, Rassendren F and Huidobro-Toro JP (2003) Histidine 140 plays a key role in the inhibitory modulation of the P2X4 nucleotide receptor by copper but not zinc. *J Biol Chem* **278**:36777-36785.
- Ennion S, Hagan S and Evans RJ (2000) The role of positively charged amino acids in ATP recognition by human P2X1 receptors. *J Biol Chem* **275**:29361-29367.
- Ennion SJ, Ritson J and Evans RJ (2001) Conserved negatively charged residues are not required for ATP action at P2X(1) receptors. *Biochem Biophys Res Commun* **289**:700-704.

MOL-010108

- Eriani G, Cavarelli J, Martin F, Ador L, Rees B, Thierry JC, Gangloff J and Moras D (1995) The class II aminoacyl-tRNA synthetases and their active site: evolutionary conservation of an ATP binding site. *J Mol Evol* **40**:499-508.
- Fabbretti E, Sokolova E, Masten L, D'Arco M, Fabbro A, Nistri A and Giniatullin R (2004) Identification of negative residues in the P2X3 ATP receptor ectodomain as structural determinants for desensitization and the Ca²⁺ sensing modulatory sites. *J Biol Chem* **279**:53109-53115.
- Freist W, Verhey JF, Stuhmer W and Gauss DH (1998) ATP binding site of P2X channel proteins: structural similarities with class II aminoacyl-tRNA synthetases. *FEBS Lett* **434**:61-65.
- Guex N and Peitsch MC (1997) SWISS-MODEL and the Swiss-PdbViewer: an environment for comparative protein modeling. *Electrophoresis* **18**:2714-2723.
- Hassinen T and Perakyla M (2001) New energy terms for reduced protein models implemented in an off-lattice force field. *J Comput Chem* **22**:1229-1242.
- He ML, Zemkova H, Koshimizu TA, Tomic M and Stojilkovic SS (2003a) Intracellular calcium measurements as a method in studies on activity of purinergic P2X receptor channels. *Am J Physiol Cell Physiol* **285**:C467-479.
- He ML, Zemkova H and Stojilkovic SS (2003b) Dependence of purinergic P2X receptor activity on ectodomain structure. *J Biol Chem* **278**:10182-10188.
- Hu B, Senkler C, Yang A, Soto F and Liang BT (2002) P2X4 receptor is a glycosylated cardiac receptor mediating a positive inotropic response to ATP. *J Biol Chem* **277**:15752-15757.
- Jiang LH, Kim M, Spelta V, Bo X, Surprenant A and North RA (2003) Subunit arrangement in P2X receptors. *J Neurosci* **23**:8903-8910.
- Jiang LH, Rassendren F, Surprenant A and North RA (2000) Identification of amino acid residues contributing to the ATP-binding site of a purinergic P2X receptor. *J Biol Chem* **275**:34190-34196.

MOL-010108

- Jones DT (1999) Protein secondary structure prediction based on position-specific scoring matrices. *J Mol Biol* **292**:195-202.
- Jones TA, Zou JY, Cowan SW and Kjeldgaard (1991) Improved methods for building protein models in electron density maps and the location of errors in these models. *Acta Crystallogr A* **47 (Pt 2)**:110-119.
- Katchalski-Katzir E, Shariv I, Eisenstein M, Friesem AA, Aflalo C and Vakser IA (1992) Molecular surface recognition: determination of geometric fit between proteins and their ligands by correlation techniques. *Proc Natl Acad Sci U S A* **89**:2195-2199.
- Khakh BS, Proctor WR, Dunwiddie TV, Labarca C and Lester HA (1999) Allosteric control of gating and kinetics at P2X(4) receptor channels. *J Neurosci* **19**:7289-7299.
- Knofel T and Strater N (2001) Mechanism of hydrolysis of phosphate esters by the dimetal center of 5'-nucleotidase based on crystal structures. *J Mol Biol* **309**:239-254.
- Koshimizu T, Koshimizu M and Stojilkovic SS (1999) Contributions of the C-terminal domain to the control of P2X receptor desensitization. *J Biol Chem* **274**:37651-37657.
- Koshimizu T, Tomic M, Koshimizu M and Stojilkovic SS (1998) Identification of amino acid residues contributing to desensitization of the P2X2 receptor channel. *J Biol Chem* **273**:12853-12857.
- Li C, Peoples RW and Weight FF (1997) Mg²⁺ inhibition of ATP-activated current in rat nodose ganglion neurons: evidence that Mg²⁺ decreases the agonist affinity of the receptor. *J Neurophysiol* **77**:3391-3395.
- Li Z, Migita K, Samways DS, Voigt MM and Egan TM (2004) Gain and loss of channel function by alanine substitutions in the transmembrane segments of the rat ATP-gated P2X2 receptor. *J Neurosci* **24**:7378-7386.

MOL-010108

- Nakazawa K, Ojima H, Ishii-Nozawa R, Takeuchi K and Ohno Y (2004) Amino acid substitutions from an indispensable disulfide bond affect P2X2 receptor activation. *Eur J Pharmacol* **483**:29-35.
- Negulyaev YA and Markwardt F (2000) Block by extracellular Mg²⁺ of single human purinergic P2X4 receptor channels expressed in human embryonic kidney cells. *Neurosci Lett* **279**:165-168.
- Newbolt A, Stoop R, Virginio C, Surprenant A, North RA, Buell G and Rassendren F (1998) Membrane topology of an ATP-gated ion channel (P2X receptor). *J Biol Chem* **273**:15177-15182.
- Nicke A, Baumert HG, Rettinger J, Eichele A, Lambrecht G, Mutschler E and Schmalzing G (1998) P2X1 and P2X3 receptors form stable trimers: a novel structural motif of ligand-gated ion channels. *EMBO J* **17**:3016-3028.
- North RA (2002) Molecular physiology of P2X receptors. *Physiol Rev* **82**:1013-1067.
- Ralevic V and Burnstock G (1998) Receptors for purines and pyrimidines. *Pharmacol Rev* **50**:413-492.
- Rettinger J, Aschrafi A and Schmalzing G (2000) Roles of individual N-glycans for ATP potency and expression of the rat P2X1 receptor. *J Biol Chem* **275**:33542-33547.
- Roberts JA and Evans RJ (2004) ATP binding at human P2X1 receptors. Contribution of aromatic and basic amino acids revealed using mutagenesis and partial agonists. *J Biol Chem* **279**:9043-9055.
- Schwede T, Kopp J, Guex N and Peitsch MC (2003) SWISS-MODEL: An automated protein homology-modeling server. *Nucleic Acids Res* **31**:3381-3385.
- Sokolova E, Skorinkin A, Fabbretti E, Masten L, Nistri A and Giniatullin R (2004) Agonist-dependence of recovery from desensitization of P2X(3) receptors provides a novel and sensitive approach for their rapid up or downregulation. *Br J Pharmacol* **141**:1048-1058.
- Tanner NK, Cordin O, Banroques J, Doere M and Linder P (2003) The Q motif: a newly identified motif in DEAD box helicases may regulate ATP binding and hydrolysis. *Mol Cell* **11**:127-138.

MOL-010108

Toyoshima C and Mizutani T (2004) Crystal structure of the calcium pump with a bound ATP analogue.

Nature **430**:529-535.

Vial C, Roberts JA and Evans RJ (2004) Molecular properties of ATP-gated P2X receptor ion channels.

Trends Pharmacol Sci **9**:487-493.

Wildman SS, King BF and Burnstock G (1999) Modulation of ATP-responses at recombinant rP2X4

receptors by extracellular pH and zinc. *Br J Pharmacol* **126**:762-768.

Xiong K, Stewart RR, Weight FF and Li C (2004) Role of extracellular histidines in antagonist sensitivity of

the rat P2X4 receptor. *Neurosci Lett* **367**:197-200.

Zemkova H, He ML, Koshimizu TA and Stojilkovic SS (2004) Identification of ectodomain regions

contributing to gating, deactivation, and resensitization of purinergic P2X receptors. *J Neurosci*

24:6968-6978.

MOL-010108

Acknowledgement: Confocal imaging was performed at the Microscopy & Imaging Core (National Institute of Child Health and Development, NIH) with the assistance of Dr. Vincent Schram.

Legends for Figures

Fig. 1. Attachment of GFP to C-terminal does not affect the expression and gating of P2X₄R. **(A)** Confocal images of GFP fluorescence in transfected HEK293 cells. Distribution of GFP without P2X₄ fusion (left panel) and P2X₄-fused GFP (right panel). **(B)** Typical patterns of ATP-induced currents in HEK293 cells expressing P2X₄ (left panel) and GFP-tagged P2X₄ (right panel) receptors. Traces shown are from different cells. Numbers below traces show mean values \pm SEM for time constants of receptor desensitization (τ_{des}) and peak amplitude (I). **(C)** ATP-induced calcium responses in GT1-7 neurons expressing P2X₄ (left panel) and P2X₄-GFP (right panel) receptors. Traces shown are means from 20 cells in a representative from 10 experiments. Numbers above traces indicate time constants of calcium signal desensitization. **(D)** Concentration-dependent effects of ATP on peak current responses in HEK293 cells expressing P2X₄ (left panel) and P2X₄-GFP (right panel). Dotted lines denote EC₅₀ values.

Fig. 2. Characterization of K190 mutant P2X₄ receptors. **(A)** The expression pattern of mutant receptors. **(B)** Typical patterns of current signals of wild type and mutant receptors in response to 100 μ M. **(C)** Current responses to two ATP concentrations. **(D)** Dose-dependent effects of ATP on peak current response by “rescue” K190R mutant. Data points are means \pm SEM values.

Fig. 3. R318 may participate in signal transduction. **(A)** Expression pattern of R318A mutant in HEK293 cells. **(B)** Mean values of peak current amplitudes in response to 100 μ M ATP. Asterisks indicate significant differences between wild type and R318A (gray bar) and R318K (black bar) mutant receptors. **(C)** Typical patterns of ATP (100 μ M) induced current signals in HEK293 cells expressing wild type and R318A (grey trace) and R318K (black trace) mutants. **(D)** Concentration-dependent effects of ATP on peak current amplitude of wild type and mutant receptor. **(E)** Representative traces of currents by wild type and mutant receptors in response to stimulation with 1 mM $\alpha\beta$ -meATP. **(F)** Concentration response curves for wild type and R318 mutants in response to stimulation with $\alpha\beta$ -meATP. Vertical dotted lines illustrate EC₅₀ values.

MOL-010108

Fig. 4. D280 may coordinate ATP binding via the magnesium at P2X₄R. **(A&B)** Loss of P2X₄R function by replacement of D280 with the non-charged Ala (A) and Gln (B) residues. (Left panels) Expression pattern of mutant receptors. (Central panels) Currents recorded in response to 100 μM ATP stimulation in wild type (black traces) and mutant (gray traces) receptors. (Right panels) Dose-dependent effects of ATP on peak current response and mean values for peak current responses in controls (black bars) and mutant receptors (grey bars). Traces shown are representative for at least 7 experiments per channel. **(C)** Rescue of function by replacing the D280 residue with negatively charged Glu. Typical patterns of current (left panel) and calcium (central panel) signals in response to 100 μM ATP of wild type (black traces) and mutant (gray traces) receptors when expressed in HEK293 (current) and GT1-7 (calcium) cells. (Right panel) Dose-dependent effect of ATP on peak current response in cells expressing mutant receptor. In all panels, bars and circles are mean ± SEM values, and asterisks indicate significant difference between controls and mutants, P<0.01. Vertical arrows indicate the moments of a transient (4 s) ATP application and horizontal bars indicate duration of sustained agonist application.

Fig. 5. Potential role of F230 residue of P2X₄R in recognition of adenine group of ATP. **(A)** Expression pattern of F230A mutant. **(B)** Typical patterns of current signals in wild type (black trace) and F230A mutant receptors (grey trace). **(C)** Dose-dependent effects of ATP on peak current response by F230A mutant. **(D&E)** Typical patterns of 100 μM ATP-induced current signals by F230W and F230Y mutants. **(F)** Dose-dependent effects of ATP on peak current response by F230W and F230Y mutants. Data points are mean ± SEM values, with N = 8 per channel. Vertical arrows indicate the moments of a transient (4 s) ATP application and horizontal bars indicate duration of sustained agonist application.

Fig. 6. Structural similarities of 185-323 ectodomain sequences of P2XRs with class II aminoacyl-tRNA synthetases. **(A)** The X-ray structure of catalytic domain of glycyl-tRNA synthetase (fragment 206-374, PDB code 1B76) with bound ATP. The crystal structures of this and two other aminoacyl-tRNA synthetases were used as templates for homology modeling of the rat P2X₄ ectodomain. **(B)** Model of rat P2X₄ ectodomain (fragment 180-326). **(C)** Residues important for ATP binding by glycyl-tRNA synthetase (PDB access code 1B76). **(D)** Residues of rat P2X₄ predicted to be involved in ATP and magnesium ion

MOL-010108

binding. Residues K190, F230, D280, and R318 of P2X₄ correspond to R220, F235, D293, and R366 in the enzyme structure, respectively. Two disulphide bridges of rat P2X₄, Cys²¹⁷-Cys²²⁷ and Cys²⁶¹-Cys²⁷⁰, are shown in orange. **(E&F)** Surface representation of ATP binding pocket of glycyl-tRNA synthetase with bound ATP (E) and ATP binding site of modeled rat P2X₄ ectodomain with docked molecule of ATP (F). Labeled amino acid residues are predicted to be involved in ATP binding. Blue and gray indicate positively charged residues, whereas orange indicates negatively charged residues.

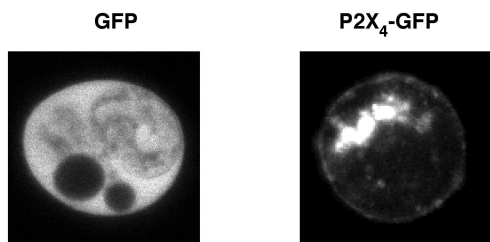
Fig. 7. Positively charged residues and detection of the phosphate chain of ATP. **(A)** Characterization of R278 mutant receptors. (Left panel) The expression pattern of mutant receptors. (Central-left panel) Typical patterns of current signals of wild type and mutant receptors in response to 100 μ M. (Central-right panel) Current responses to two ATP concentrations. (Right panel) Dose-dependent effects of ATP on peak current response by “rescue” mutants. Data points are means \pm SEM values, with N = 7. **(B)** Mutation of H286 removes extracellular pH sensitivity of receptor expressed in HEK293 cells. (Left panel) Typical currents of wild type (bottom trace) and mutant (upper trace) receptors in response to 3 μ M ATP stimulation. (Central panel) Comparison of the peak current amplitude for wild type and mutant receptors in response to 3 μ M ATP at pH 8.0 (white bars) and 6.5 (black bars). (Right panel) Dose-dependent effects of ATP on peak current response by H286A mutant. Vertical arrows indicate initiation of a transient (4 s) ATP application and horizontal bars indicate duration of sustained agonist applications.

MOL-010108

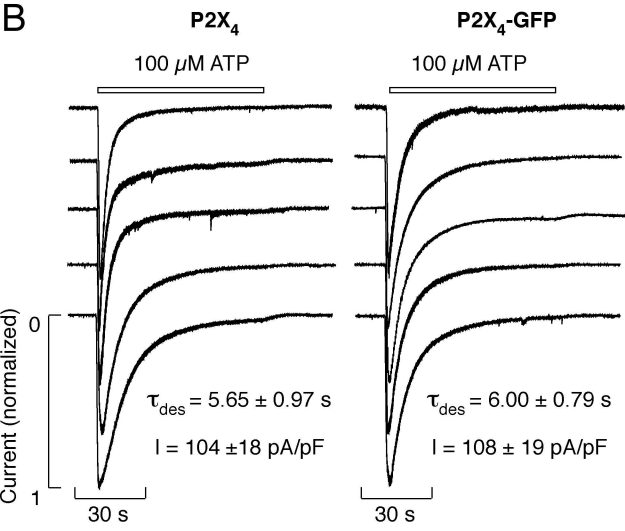
Table 1. Characterization of ATP-induced currents in HEK293 cells expressing wild type and mutant rat P2X₄ receptors. Peak current values and τ_{des} values were derived from responses to 100 μ M ATP. Data shown are means \pm SEM; * $p < 0.01$ vs. wild type channel. Number of experiments per group varied between 5 and 15.

P2X ₄ Channels	EC ₅₀ values (μ M)	Peak current amplitude (pA/pF)	τ_{des} (s)
Wild type	3.0 \pm 0.5	82.9 \pm 9.4	5.7 \pm 0.6
K190A	> 5000	0.9 \pm 0.4	-
K190R	6.7 \pm 0.6*	44.7 \pm 7.2*	5.9 \pm 1.1
K197A	3.8 \pm 0.8	32.4 \pm 3.1*	4.8 \pm 0.8
F230A	> 5000	1.5 \pm 0.4*	-
F230W	3.9 \pm 0.6	67.1 \pm 8.3	6.1 \pm 1.2
F230Y	5.9 \pm 1.3	67.7 \pm 11.7	6.7 \pm 2.2
K258A	3.8 \pm 1.4	70.4 \pm 9.9	4.7 \pm 0.8
R278A	> 5000	3.7 \pm 0.6*	-
R278K	1.9 \pm 0.3	43.4 \pm 1.7*	4.5 \pm 0.6
D280A	> 5000	3.7 \pm 0.9*	-
D280Q	> 5000	1.4 \pm 0.5*	-
D280E	3.6 \pm 0.4	41.1 \pm 9.8*	6.4 \pm 0.7
H286A	3.7 \pm 0.7	38.8 \pm 6.2*	3.7 \pm 0.7
N287A	5.8 \pm 0.8	34.9 \pm 4.9*	7.3 \pm 1.4
R318A	59 \pm 9.5*	36.5 \pm 8.8*	6.6 \pm 1.4
R318K	1.2 \pm 0.3	56.3 \pm 19.4	5.8 \pm 0.6

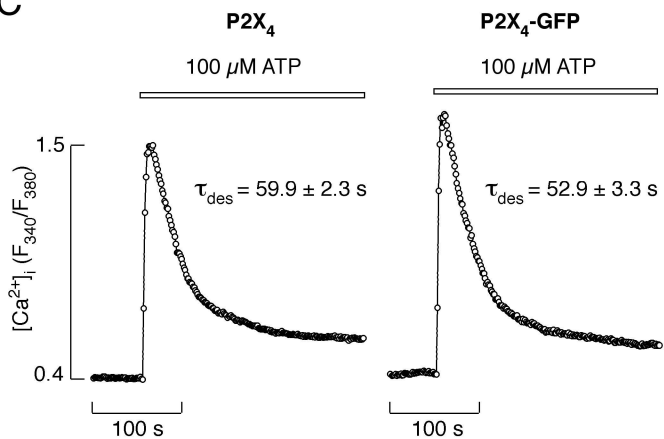
A



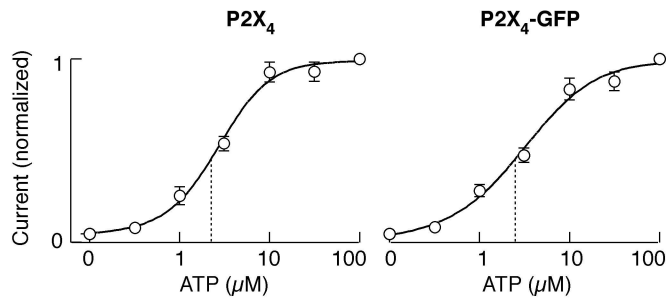
B



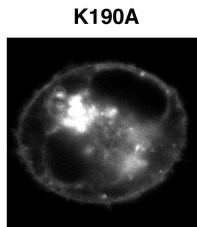
C



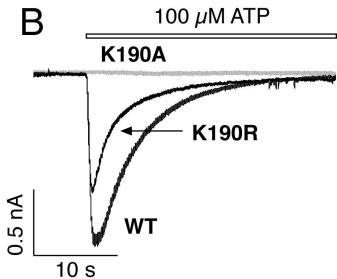
D



A

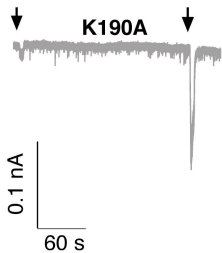


B

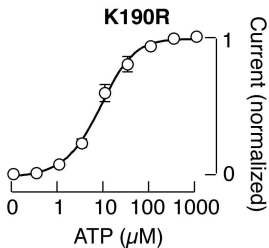


C

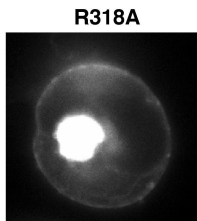
100 μ M ATP 5 mM ATP



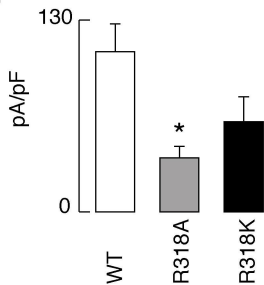
D



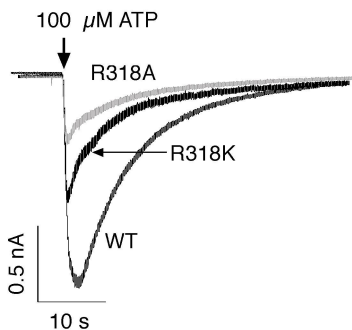
A



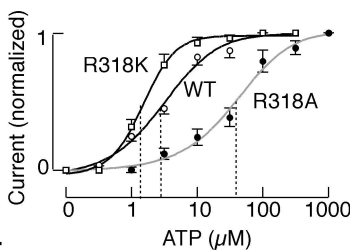
B



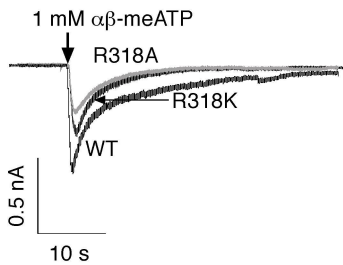
C



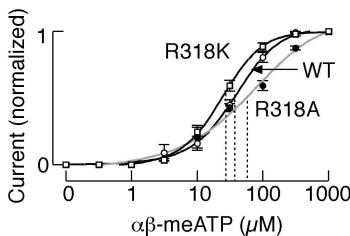
D

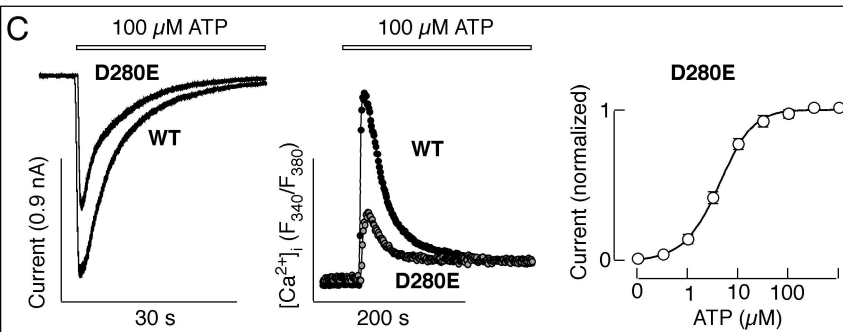
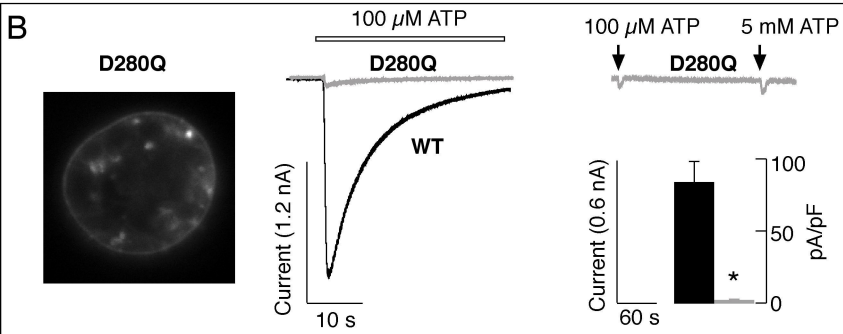
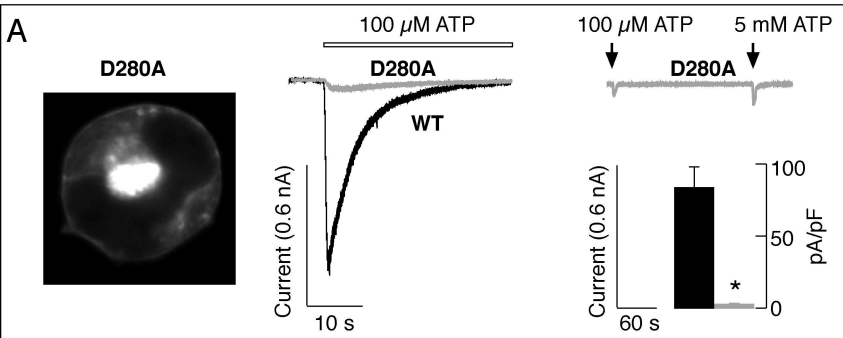


E

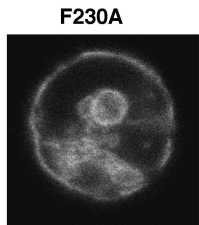


F

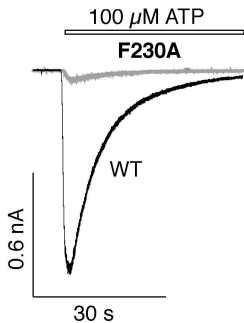




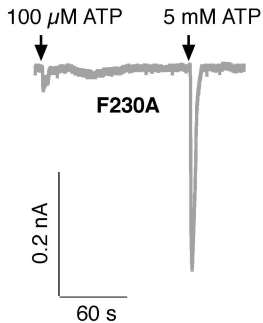
A



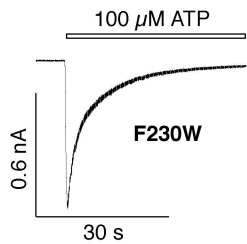
B



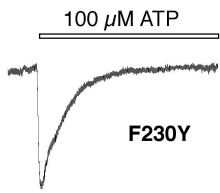
C



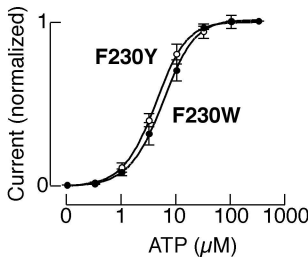
D



E

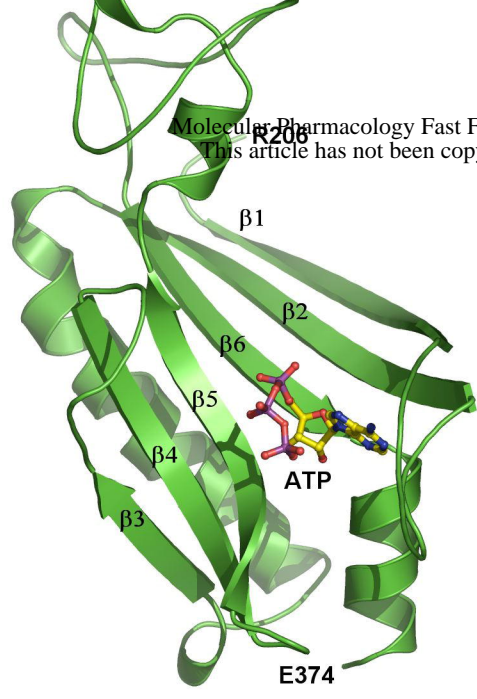


F

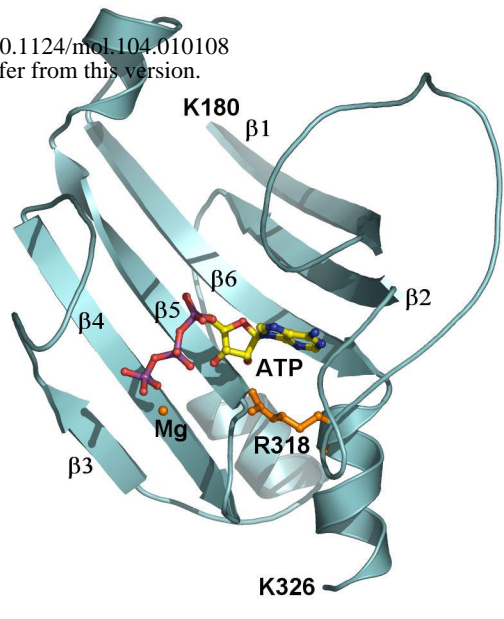


A

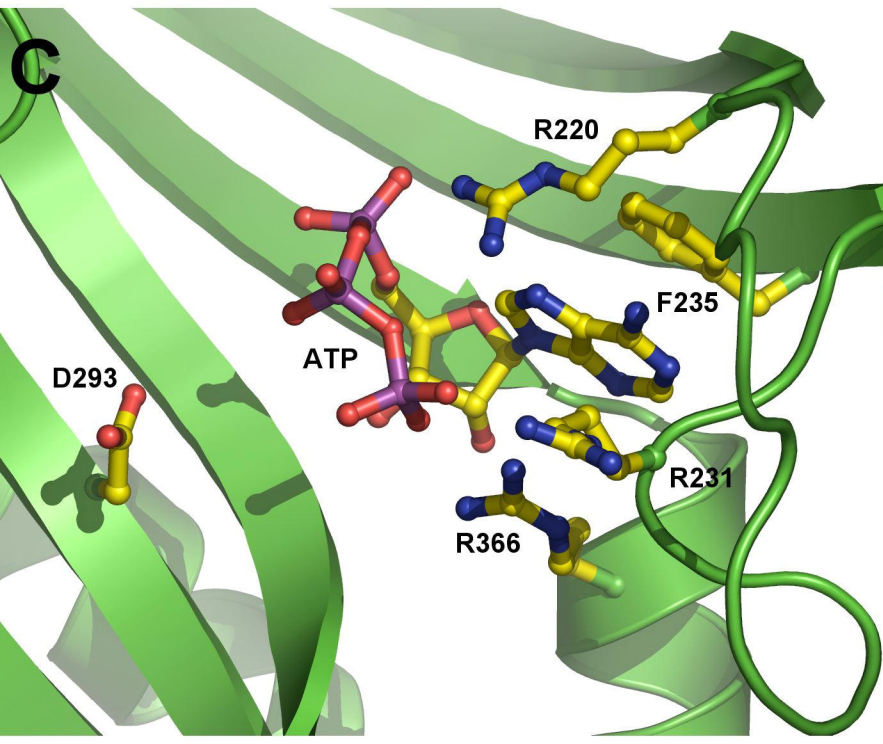
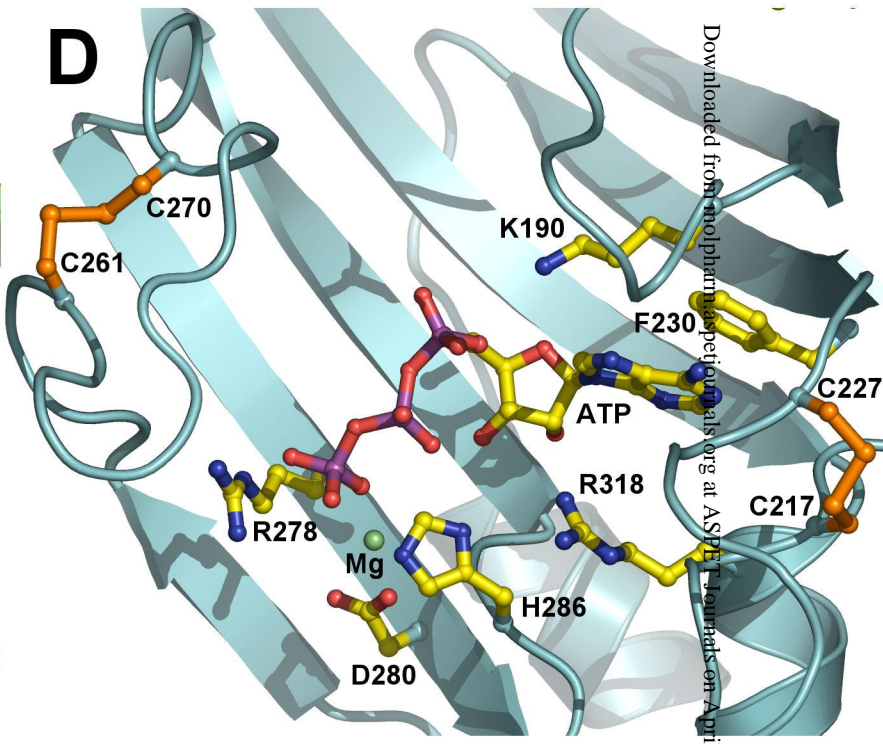
Glycyl-tRNA Synthetase
fragment 206-374

**B**

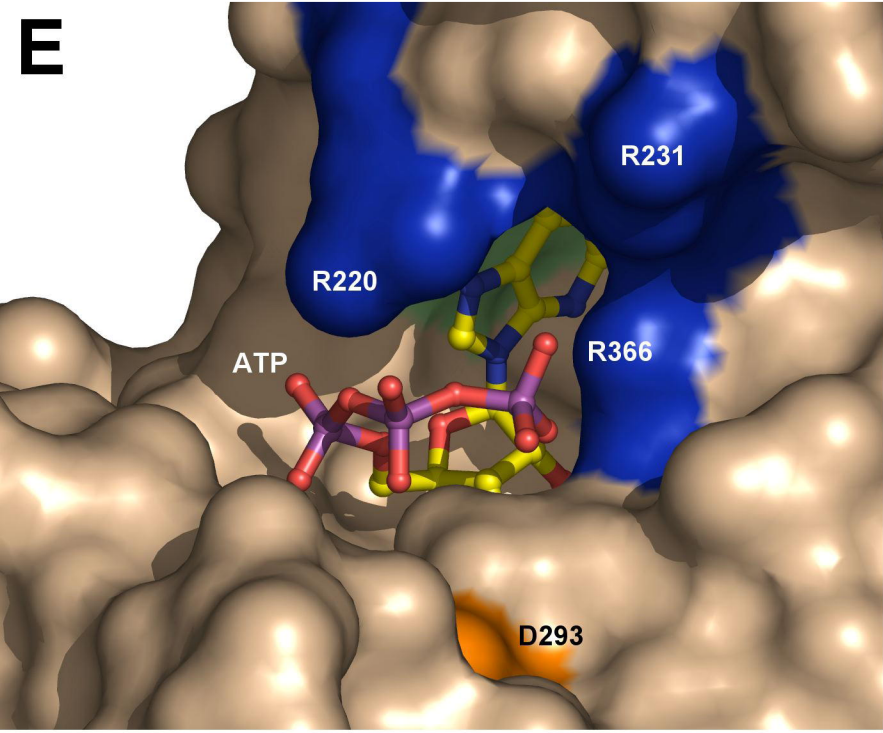
Model of rat P2X4 ectodomain
fragment 180-326



Molecular Pharmacology Fast Forward. Published on January 4, 2005 as DOI: 10.1124/mol.104.010108
This article has not been copyedited and formatted. The final version may differ from this version.

C**D**

Downloaded from molpharm.physioliasa.org at ASPET Journals on April 20, 2024

E**F**